16th World Conference on Earthquake Engineering, 16WCEE 2017
Santiago Chile, January 9th to 13th 2017
Paper N° 4638 (Abstract ID)
Registration Code: S-W1464756295

SEISMIC LOSS ESTIMATE OF SINGAPORE UNDER A DETERMINISTIC SUMATRAN EARTHQUAKE SCENARIO

W. Du[(1)], T.C. Pan [(2)],and M.Y. Walling[(3)]

[(1)] Research Fellow, Institute of Catastrophe Risk Management, Nanyang Technological University, Singapore, wqdu@ntu.edu.sg
[(2)] Executive Director and Professor, Institute of Catastrophe Risk Management and School of Civil and Environmental Engineering, Nanyang Technological University, Singapore, TCPan@pmail.ntu.edu.sg
(3) Research Fellow, Institute of Catastrophe Risk Management, Nanyang Technological University, Singapore, mywalling@ntu.edu.sg

Abstract

Evaluation of seismic risk for large cities has become increasingly important due to the concentration of exposures resulting from their dense population and rapid economic growth. Singapore is a modern city located in a low-to-moderate seismicity zone. It has frequently felt shakings by long-distance major earthquakes originated from the Sumatra region. In this study, the seismic loss estimates are conducted for Singapore considering a deterministic earthquake scenario. A set of ground motions is simulated for a Sumatran strike-slip M_w 7.7 earthquake scenario. To quantify the site amplification effects of Singapore, 555 soil profiles which include shear-wave velocity and unit weight profiles are used. The collected boreholes can be grouped as ground types B, C and D, respectively. One-dimensional equivalent-linear analysis is performed using the SHAKE program. The main Singapore terrain is uniformly gridded in 200 m x 200 m squares, which result in 19,276 cells in total. Kriging techniques are then utilized to estimate surface ground motion intensity values at each cell. The building inventory data consist of about 123,000 buildings of 1 to 15 stories. For each building category, the structural losses can be estimated based on the capacity spectrum and fragility procedures in HAZUS-MH. The estimated structural losses of Singapore are about 0.5% of the total exposure. Since most Singapore buildings have been designed according to the BS code with the requirement of notional horizontal load, it is important to understand the seismic performance of buildings under the postulated scenarios of major long-distance earthquakes. This approach can also be applied to other major urban centers with significant exposures in a low to moderate seismicity region.

Keywords: Urban loss estimation; Ground motion simulation; Site response analysis; Singapore.

1. Introduction

Evaluation of seismic risk for large cities has become more important due to the concentration of exposures resulting from the dense population and rapid economic growth. For instance, the 2010 Haiti earthquake, which occurred about 15 km away from the Port-au-Prince city, caused a catastrophe with more than 200,000 deaths and about US$ 8.1 billion loss [1].

To accurately evaluate the seismic losses of spatially-distributed portfolios, it is important to generate representative ground motion intensity maps (e.g., peak ground acceleration (PGA) map) for given earthquake scenarios. The simplest and most widely method is associated with ground motion prediction equations (GMPEs). At each location, the median intensity measure (IM) value is estimated via a GMPE with input parameters (e.g., magnitude, source-to-site distance, site condition, fault type). Apart from GMPEs, spatial correlation models of IMs developed by some scholars [e.g., 2-5] should also be considered. The influence of considering spatial correlations of IMs in earthquake risk assessment for specific structures or infrastructures has been widely investigated [e.g., 6-7]. Except for the GMPE-based method, another commonly used method is to generate surface ground motion IMs using simulated ground motions [8]. At each location, ground motions are simulated with specific magnitude, distance, azimuth angles and site conditions, generally using the stochastic finite-fault technique [9]. The process of simulating ground motions is usually time consuming.

Although there were no earthquake-induced damages reported previously in Singapore, the seismic risk should be well quantified due to the neighboring Great Sumatran fault [10]. Currently there are no available GMPEs to predict surface ground motions in Singapore, making it difficult to use the GMPE-based method. It is also not convenient to generate simulated ground motions at each location due to the territorial scale. Therefore, this study focuses on developing an alternative method for seismic structural losses of Singapore. The procedures can be simplified as: first, a number of well-distributed boreholes are collected. For an earthquake scenario with simulated bedrock ground motions, the surface ground motion at each borehole location can be predicted by site response analysis. Second, the spatial covariance models of IMs for each ground type are developed using the IM values at borehole locations. Then approximate estimations of IMs at un-sampled locations can be assigned by kriging techniques [11]. Finally, based on the distribution of surface ground motions, a comprehensive seismic loss evaluation of Singapore can be implemented following the standard methods such as HAZUS-MH.

2. Regional Seismology of Singapore

Singapore is a modern city located in a low-to-moderate seismicity zone. It frequently felt the shakings by long-distance giant earthquakes originated from the Sumatra fault zone [10]. The main seismic sources in this region consist of Sumatra subduction fault and Sumatra strike-slip fault. In particular, the Sumatra megathrust, which was formed by the subduction of Indian-Australian plate underneath south-eastern Eurasian plate, is well known to generate great earthquakes (M_w>8). The largest earthquake occurred in this subduction fault is the devastating M_w 9.1 Aceh-Andaman earthquake in 2004.

The Sumatran strike-slip fault lies about 250 km northeast of the Sunda trench (Fig. 1). It has been identified as a 1,900-km long right-lateral strike-slip fault. The Sumatran fault is divided in 20 major segments and the length of the faults ranges from 35 km to 200 km. More than a dozen of large earthquakes (larger than magnitude 7) have occurred historically along this fault. The largest earthquake magnitude occurred at the Angkola segment (M_s = 7.7) in 1892, followed by the Sumani segment (M_s = 7.6) in 1943.

Although the Sumatran megathrust is more capable of producing great earthquakes than the Sumatran fault, it has been studied that the Sumatran fault probably gives a stronger impact (larger amplitudes of motions) to Singapore, due to its closer source-to-site distance [12, 13]. Therefore, this study only focuses on the seismic hazard resulting from the Sumatran strike-slip fault. Then a M_w 7.7 earthquake event in the Sumani segment can be regarded as the scenario earthquake occurred in the Sumatran strike-slip fault zone.

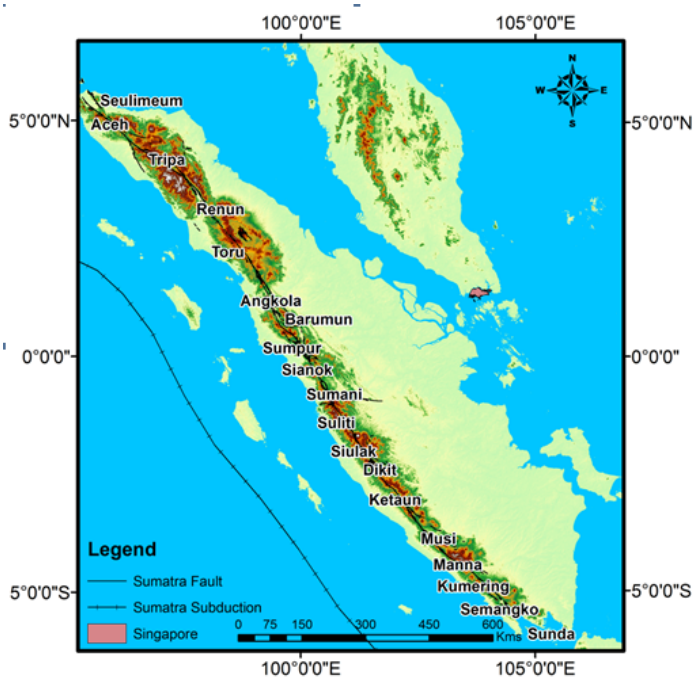

Fig. 1 Regional tectonic settings of Sumatra megathrust and the Sumatran-fault segments.

3. Ground Motion Simulations

The synthetic ground motions are simulated using a stochastic finite-fault model [14]. This method models the rupture initiation at one point of the plane (hypocenter) and it propagates radially to all parts of the subfaults with a certain rupture velocity. For a given site, the resulted ground motions generated by the rupture of each subfault are superimposed with appropriate time lags, and then the final ground motion from the whole fault plane can be obtained. The regional crustal velocity structure model is taken from the CRUST 2.0 [15], which is a 2°×2° global crustal model. The detailed properties of the crustal structure and sedimentary hard-rock of Sumatra are summarized in Table 1. The Green's functions for the layered crustal structure can provide proper phasing of body and surface waves.

Table 1 Structure of crust and sedimentary hard rock for Sumatra region.

*Layer	H (km)	V_p (km/s)	V_s (km/s)	ρ (t/m^3)	Q_p	Q_s
Sedimentary hard-rock	0.2	3.72	1.92	2.37	200	100
Upper crust	9.6	6.0	3.4	2.7	500	250
Middle crust	9.5	6.6	3.7	2.9	700	350
Lower crust	9.1	7.2	4.0	3.1	900	450
Mantle	–	8.14	4.64	3.37	1000	500

*: H: layer thickness; V_p: P-wave velocity; V_s: S-wave velocity; ρ: mass density; Q_p: quality factor of *P*-wave; Q_s: quality factor of *S*-wave.

The ruptured area for the M_w 7.7 strike-slip earthquake in the Sumani segment is set as 140 km × 21 km. The size of each subfault is 7 km × 7 km, resulting in 60 subfaults in total. The strike and dip angles of this fault are N30°W and 87°, respectively. The epicenter of the event is assumed to be at the center of the defined fault

rupture area. The slips of the subfaults are lognormally distributed with a coefficient of variance as 0.2. The average slip is assigned as 2.47 m, which is computed using the empirical slip model proposed by Somerville et al [16]. Two asperities are also considered in the slip distribution, which takes 20% of the total area. The average slip in the asperity area is assigned as 6.1 m.

The ground motions for Singapore can be simulated using the introduced finite-fault model and source parameters. The mainland of Singapore is divided into 1 km × 1 km grids and the center of each grid is regarded as the site to measure the epicentral distance. The simulation process is only performed for grid cells with soil profiles included, resulting in 120 sets of ground motions for the strike-slip M_w 7.7 event. The epicentral distances of the 120 sites vary from 405 km to 452 km. The computed response spectral accelerations for the radial and transverse components of the simulated ground motions, along with the mean as well as 'mean ± 1 standard deviation' spectral curves, are shown in Fig. 2. The *Sa* values of the transverse component are much higher than those of the radial component. Thus, the simulated motions of the transverse component will be used as input motions for the subsequent site response analysis.

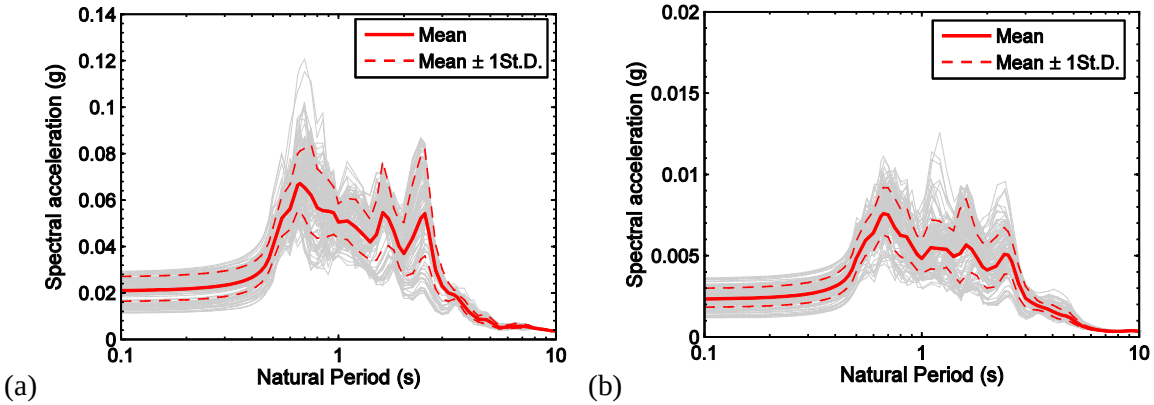

Fig. 2 Computed response spectra of the simulated ground motions (bedrock layer) for (a) transverse direction and (b) radial direction.

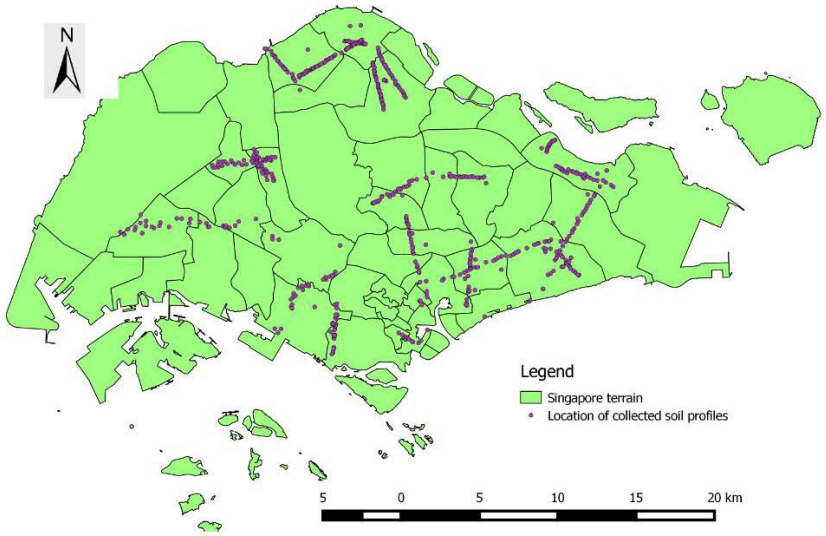

Fig. 3 Spatial distribution of sites with collected soil profiles

4. Seismic Loss Estimation of Singapore

4.1 Site response with SHAKE program

Totally 555 soil profiles are collected in Singapore. The data sets provide the description of soil layers, including the unit weight and shear wave velocity (Vs) profiles. Fig. 3 displays the locations of these sites, using a geographical information system (GIS) platform. It can be observed that the sites are generally well scattered across the building inventory of Singapore. The SHAKE program [17] is used to compute the surface ground motions at the 555 sites. One-dimensional analysis (upward propagation of seismic waves) is performed by this program, and an equivalent linear approximation method is implemented in a frequency domain. As shown in Fig. 4, the empirical modulus-reduction and damping models proposed by Vucetic and Dobry [18] are adopted to model the soil nonlinearity. It has been studied that the SHAKE program can fairly predict the seismic site response, and therefore it is widely used in geotechnical earthquake engineering [19].

Site response analyses are then performed for these sites using simulated ground motions for the strike-slip M_w 7.7 earthquake. Fig. 5 (a), (b) and (c) show the surface response spectra for all the sites belonging to ground types B, C and D, respectively. The 'mean' as well as 'mean plus one standard deviation' spectra curves of 114, 251, 190 soil profiles for ground types B, C, D respectively are also plotted in each figure. As expected, the sites in ground type B result in smallest amplification effect. The computed surface IM values can be regarded as the sampled data at each site, which can be further used to estimate IMs at un-sampled locations.

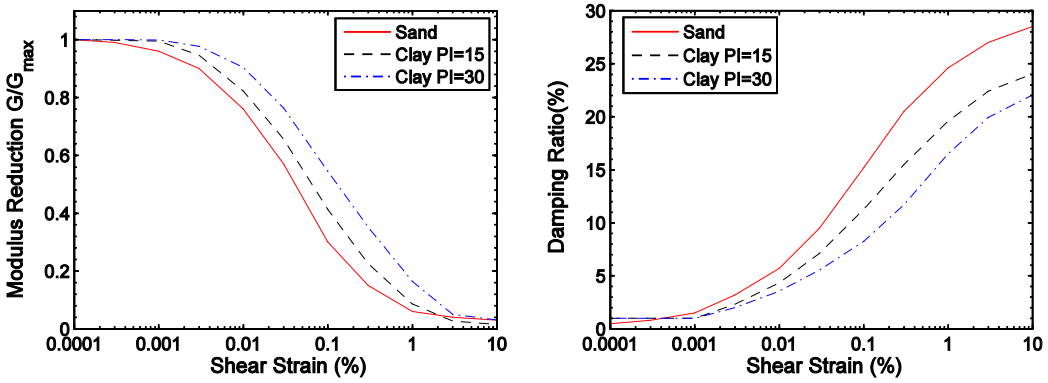

Fig. 4 Examples of shear modulus reduction and damping ratio curves used for site response analysis [16].

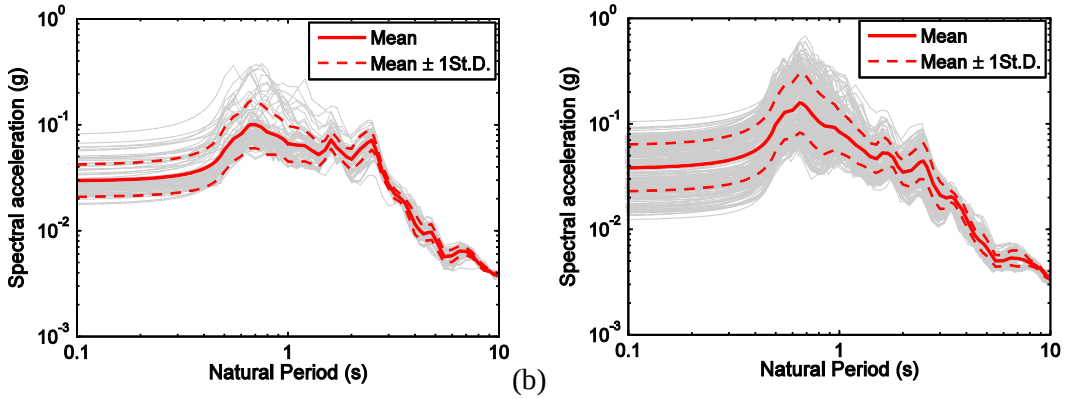

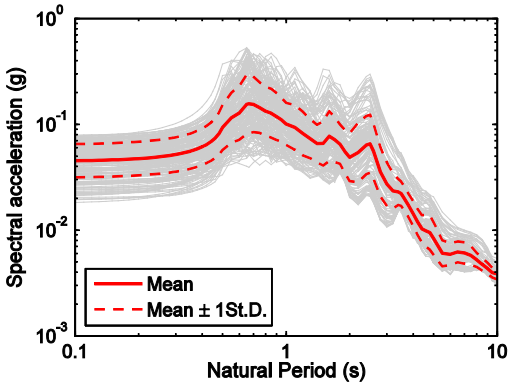

(c)

Fig. 5 (a), (b) and (c) Surface spectral accelerations computed by SHAKE using the simulated M_w 7.7 ground motions for ground types B, C and D, respectively.

4.2 Kriging technique

Spatial correlation modeling and kriging techniques are briefly introduced in this section. These geostatistical tools are necessary to estimate the surface IM values at un-sampled locations (without soil profile information).

In a random field (RF), spatial variability can be represented using pairs of data for a given $\boldsymbol{h}$ (separation distance and direction). Semivariogram γ is a widely used measure to quantify the dissimilarity between data separated by a vector distance $\boldsymbol{h}$ [11]:

$$\gamma(\boldsymbol{h}) = \frac{1}{2} Var\left[Z(\boldsymbol{u}) - Z(\boldsymbol{u}+\boldsymbol{h})\right] = \frac{1}{2} E\left[(Z(\boldsymbol{u}+\boldsymbol{h}) - Z(\boldsymbol{u}))^2\right] \quad (1)$$

where $Z(\boldsymbol{u})$ and $Z(\boldsymbol{u}+\boldsymbol{h})$ denote random variables at locations $\boldsymbol{u}$ and $\boldsymbol{u}$+$\boldsymbol{h}$, respectively. Under second-order stationary conditions, the relationship between semivariograms and covariance functions is theoretically constructed as [11]:

$$\gamma(\boldsymbol{h}) = C(0) - C(\boldsymbol{h}) \quad (2)$$

The empirical semivariograms can be estimated as:

$$\tilde{\gamma}(\boldsymbol{h}) = \frac{1}{2\left|N(\boldsymbol{h})\right|} \sum_{\alpha=1}^{N(h)} \left[z(u_\alpha + \boldsymbol{h}) - z(u_\alpha)\right]^2 \quad (3)$$

where $\tilde{\gamma}(\boldsymbol{h})$ represents empirical semivariograms; $N(\boldsymbol{h})$ is the number of data pairs within this distance bin $\boldsymbol{h}$; $z(u_\alpha + \boldsymbol{h})$ and $z(u_\alpha)$ represent the α_{th} data pair separated by distance $\boldsymbol{h}$. If the random field is isotropic and second-order stationary, the vector $\boldsymbol{h}$ can be replaced by a scalar distance variable $h = \|\boldsymbol{h}\|$.

Empirical semivariograms $\tilde{\gamma}(h)$ consist of a set of discrete values for different distance h. Some basic models, such as spherical, Gaussian and exponential models are commonly used to fit the empirical data. The exponential model with nugget effect is adopted in this paper with following function as:

$$\tilde{\gamma}(h) = \begin{cases} c_0 + (c - c_0)\left[1 - \exp(-3h/b)\right] & h > 0 \\ 0 & h = 0 \end{cases} \quad (4)$$

where c_0, c and b are the *nugget*, *sill* and *range* of the semivariograms, respectively. The *nugget* c_0 can be interpreted as the measurement error with the sample. The *range* b is defined as at the separation distance h, in which $\tilde{\gamma}(h)$ equals 95% of the *sill* c. The parameters c_0, c and b can be obtained by the ordinary or weighted least square regression.

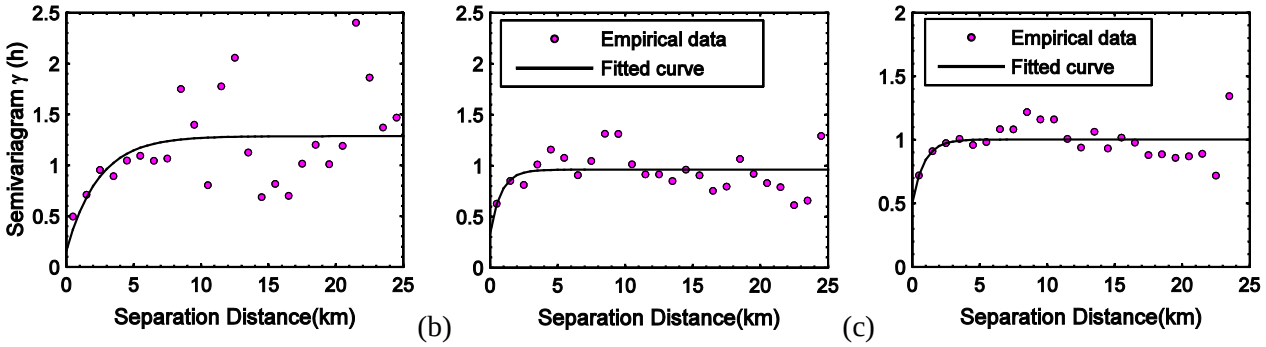

Fig. 6 (a), (b) and (c): Empirical semivariograms and fitted curves for ground types B, C and D, respectively. The estimated surface PGA ordinates by site response computations are used as empirical data.

Following the above introduced information, the semivariograms with respect to separation distance *h* for PGA are shown in Fig. 6 for ground types B, C and D, respectively. The fitted exponential curves are also shown in each plot. It can be seen that the curves fit the empirical data reasonably well. Therefore, as long as the *nugget* c_0, *sill c* and *range b* are obtained, the covariance structure *C*(*h*) can be fully quantified. The covariance function is necessary to estimate the values at un-sampled locations via a kriging method.

The kriging approach enables us to estimate random variables at unknown locations. The kriging method represents a group of generalized least-squares regression for spatial interpolations [11]. There are several important kriging paradigms such as simple kriging, ordinary kriging and kriging with a trend models. Among these estimators, the simple kriging estimators are closer to the global mean value, while the ordinary kriging can better account for local data fluctuations. In general, the ordinary kriging can provide better unbiased local estimates.

The ordinary kriging estimator $\tilde{Z}(\boldsymbol{u})$ at location $\boldsymbol{u}$ can be expressed as a linear combination of the sampled data $Z(\boldsymbol{u}_\alpha)$:

$$\tilde{Z}(\boldsymbol{u}) = \sum_{\alpha=1}^{K} \lambda_\alpha(\boldsymbol{u}) \cdot Z(\boldsymbol{u}_\alpha) \tag{5}$$

where $\lambda_\alpha(\boldsymbol{u})$ is an assigned weight of the α_{th} sampled location at an unknown location $\boldsymbol{u}$; *K* is the number of sampled data; and $Z(\boldsymbol{u}_\alpha)$ denotes the sampled values located at $\boldsymbol{u}_\alpha$. The weights $\lambda_\alpha(\boldsymbol{u})$ can be determined by minimizing the error variance $\mathrm{Var}(\tilde{Z}(\boldsymbol{u}) - Z(\boldsymbol{u}))$. To get unbiased estimation, the sum of kriging weights should be equal to 1, namely $\sum_{\alpha=1}^{K} \lambda_\alpha(\boldsymbol{u}) = 1$.

The minimization of the error variance needs the definition of a Lagrangian L($\boldsymbol{u}$), and thus the aforementioned constraints can be transferred as:

$$\begin{cases} \sum_{\beta=1}^{K} \lambda_\beta(\boldsymbol{u}) \cdot C(\boldsymbol{u}_\alpha - \boldsymbol{u}_\beta) + \mu(\boldsymbol{u}) = C(\boldsymbol{u}_\alpha - \boldsymbol{u}) \\ \sum_{\beta=1}^{K} \lambda_\beta(\boldsymbol{u}) = 1 \end{cases} \tag{6}$$

where $\alpha, \beta = 1, 2, \ldots, K$; $\mu(\boldsymbol{u})$ means a Lagrange parameter; and $C(\boldsymbol{u}_\alpha - \boldsymbol{u})$ is the covariance function (as shown in Eq. (2)). The kriging weights $\lambda(\boldsymbol{u})$ can be obtained by solving Eq. (6). Once $\lambda(\boldsymbol{u})$ is solved, $\tilde{Z}(\boldsymbol{u})$ at un-sampled location $\boldsymbol{u}$ can be determined via Eq. (5).

4.3 Ground motion intensity maps

The site response results as well as geostatistical techniques can be used to generate surface PGA and *Sa* maps of Singapore. Kriging within strata is appropriate for such purpose, and the geological ground types can be used for stratifications. First, terrain of Singapore is firstly divided into 19,276 cells with a 0.2 km × 0.2 km grid, and then they are stratified according to the ground type classifications. Second, in each stratum, the ordinary kriging method can be used to estimate the values of IMs at un-sampled locations.

Fig. 7 (a) shows the realization of the PGA map for the strike-slip M_w 7.7 event. They are generated using the computed surface ground motions at 555 sites in conjunction with the kriging within strata. The higher PGA values can be observed at the surrounding grids of some boreholes, at which significant site amplifications are computed. Besides, there is a notable distinction at the ground type boundaries, which is not surprising due to the stratifications. Similarly, the *Sa* maps for other periods across the Singapore terrain can be generated. The corresponding *Sa* curves at each grid can be used to estimate seismic losses in the next section.

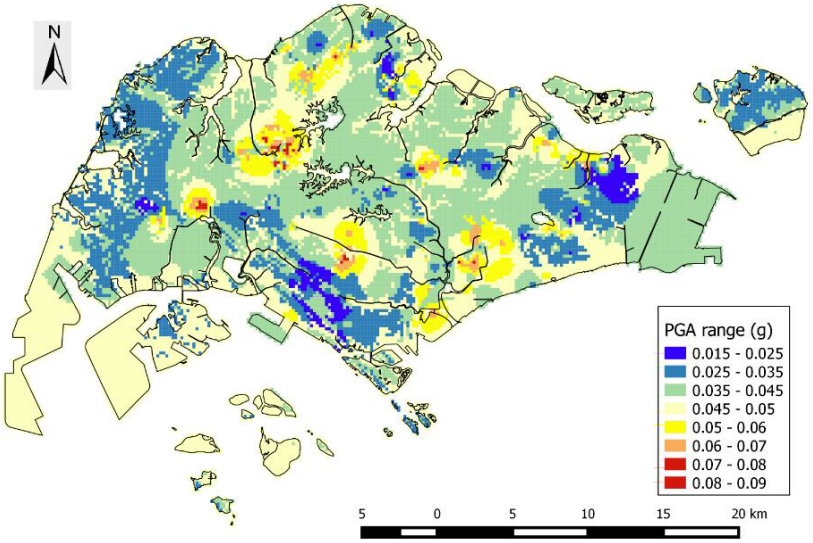

Fig. 7 Surface PGA map of Singapore using kriging within strata. The gridded cells are classified into different strata by geological ground types. The simulated M_w 7.7 ground motions are used for this computation.

Table 2 Building inventory classifications for buildings of Singapore defined by HAZUS-MH

Building Index	Description	Range of Storeys	Typical Storey	Seismic Design Level
RM2L	Reinforced Masonry Bearing Walls	1-3	2	Low-Code
S2L	Steel Frame	1-3	2	Low-Code
C1L	RC Moment Frame	1-3	2	Low-Code
C1M	RC Moment Frame	4-7	6	Low-Code
C1H	RC Moment Frame	8-15	12	Low-Code
C2H	RC Shear wall	8-15	12	Low-Code

RC: reinforced concrete.

4.4 Estimated structural losses

The building inventory data of Singapore used in this study consists of 122,825 individual buildings with stories ranging from 1 to 15. Based on the building classifications in HAZUS-MH, the buildings of Singapore can be classified into several main types, as shown in Table 2. most buildings in Singapore were designed based on the BS8110 code [20], which can be classified as a low-code seismic design level.

The building capacity curves and fragility curves at the low-code level provided in HAZUS-MH should be selected for each building type. The capacity curves plot buildings' load resistance with respect to lateral displacement, quantifying the building displacement response in the elastic and inelastic range. The fragility curves represent the probability of exceeding a given damage state as a function of spectral displacements. Four damage states, namely, *slight*, *moderate*, *extensive* and *complete* are usually considered for loss estimation [21]. The default capacity and fragility curves at the low-code level provided in HAZUS-MH are adopted in this study. For each building, the structural loss can be estimated following standard procedures of HAZUS.

Table 3 displays the number of damaged buildings for low-, mid- and high-rise structures of Singapore. It can be seen that most buildings of Singapore would not suffer any damage under the considered Sumatran M_w 7.7 earthquake scenario. Table 4 shows the summary of the estimated structural losses in Singapore. The greatest losses are resulted from high-rise buildings. This may be due to the spectral shape of the obtained surface ground motions, as shown in Fig. 5. Since the long-distance ground motions mainly consist of long-period seismic waves, which would result in more responses of the high-rise buildings. Besides, it is not surpsring that most structural losses came from buildings located on soft soils (ground types C, D and S_1), due to the significant site effect. The total structural losses are approximately 0.5% of the total exposure value.

Fig. 8 shows the distribution of the aggregated structural losses in the geographical unit level (0.2 km×0.2 km). It can be seen that the estimated building losses in Singapore are mostly concentrated in the southeast region, namely, the downtown area of Singapore. This is expected, since a large number of buildings are built on soft soils in this region. Therefore, more attention should be paid to the seismic risk assessment and mitigation of this region in future.

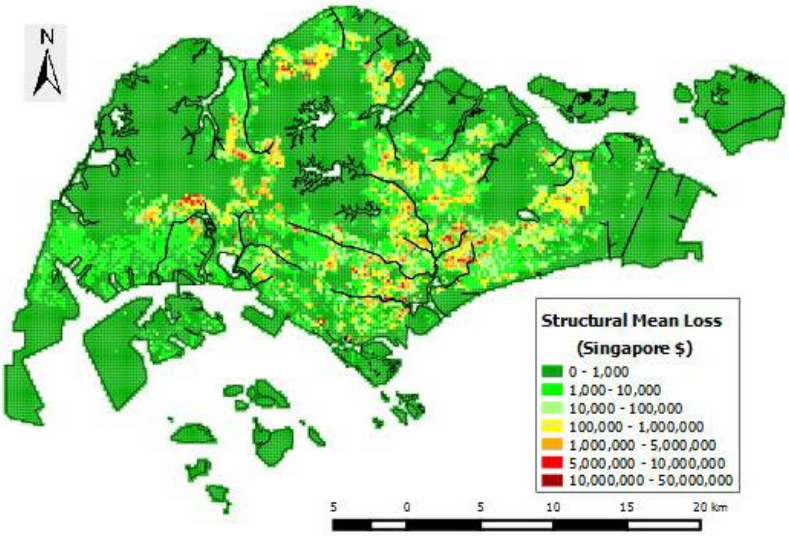

Fig. 8 Structural loss map of Singapore for the considered Sumatran M_w 7.7 event

Table 3 Number of damaged buildings in Singapore subjected to the Sumatran strike-slip M_w 7.7 event.

Building Type	Damage state	No. of damaged buildings
Low-rise (1-3 story)	Slight	281
	Moderate	40
	Extensive & Complete	0
	Total no. of buildings	107409
Mid-rise (4-7 story)	Slight	44
	Moderate	14
	Extensive & Complete	0
	Total no. of buildings	8215
High-rise (8-15 story)	Slight	445
	Moderate	314
	Extensive	68
	Complete	0
	Total no. of buildings	7201

Table 4 Summary of the computed building losses in Singapore

		Structural losses (million-S$)	Total exposure (million-S$)	Ratio (%)
Building class	Low-rise	13.7	156,786	0.01
	Mid-rise	46.0	131,340	0.04
	High-rise	2,699.3	263,350	1.02
Ground type	GT A	0.0	36.2	0.00
	GT B	349.8	133,364	0.26
	GT C	1,016.5	242,006	0.42
	GT D&S_1	1,392.7	176,069	0.79
-	Total	2,759.0	551,476	0.50

5. Conclusion

A simplified urban loss estimation method based on the combination of ground motion simulation, site response and geostatistical analysis was presented in this paper. Take the worst-case earthquake (M_w 7.7) from the Sumatran strike-slip fault as a deterministic scenario of Singapore, it has been demonstrated how to generate ground motion intensity fields using site response analyses, spatial covariance models and kriging techniques. Then the capacity and fragility curves provided by HAZUS-MH are adopted for each building type of Singapore. The seismic structural losses of Singapore are then estimated following the HAZUS-MH approaches.

Under the deterministic M_w 7.7 earthquake scenario, the majority of buildings (more than 99%) in Singapore would experience none or slight damage, and a very limited number of buildings would suffer moderate or extensive damage. Although only a small percentage of buildings are exposed to moderate damage state, the estimated total structural loss is about 0.6% of Singapore GDP in 2014. It has been observed that the buildings in the southeast part of Singapore are susceptible to economic losses subjected to seismic shakings. The results demonstrate the potentially high seismic losses of Singapore when large and infrequent distant Sumatran earthquakes occur.

This method is applicable for cities where seismic site effect is significant. It can be regarded as an alternative method, which might hopefully provide new insights into seismic risk evaluation or loss estimates of urban regions.

Acknowledgements

The authors acknowledge financial supports provided by the Ministry of Home Affairs and the Monetary Authority of Singapore for this work.

References

[1] Cavallo E, Powell A, Becerra O (2010): Estimating the direct economic damages of the earthquake in Haiti. *The Economic Journal*, **120** (546), F298-F312.

[2] Jayaram N, Baker JW (2009): Correlation model for spatially distributed ground-motion intensities. *Earthquake Engineering & Structural Dynamics*, **38**,1687-1708.

[3] Esposito S, Iervolino I. (2011): PGA and PGV spatial correlation models based on European multievent datasets. *Bulletin of the Seismological Society of America* 2011, **101**(5), 2532-2541.

[4] Du W, Wang G (2013): Intra-event spatial correlations for cumulative absolute velocity, Arias intensity, and spectral accelerations based on regional site conditions. *Bulletin of the Seismological Society of America*, **103**(2A), 1117-1129.

[5] Wang G, Du W (2013): Spatial cross-correlation models for vector intensity measures (PGA, Ia, PGV, and SAs) considering regional site conditions. *Bulletin of the Seismological Society of America*, **103**(6), 3189-3204.

[6] Goda K, Hong HP (2009): Deaggregation of seismic loss of spatially distributed buildings. *Bulletin of Earthquake Engineering*, **7**(1), 255-272.

[7] Du W, Wang G (2014): Fully probabilistic seismic displacement analysis of spatially distributed slopes using spatially correlated vector intensity measures. *Earthquake Engineering & Structural Dynamics*, **43**(5), 661-679.

[8] Liu TJ, Hong HP (2015): Application of spatially correlated and coherent records of scenario event to estimate seismic loss of a portfolio of buildings. *Earthquake Spectra*, **31**(4), 2047-2068.

[9] Ghofrani H, Atkinson GM, Goda K, Assatourians K (2013): Stochastic finite−fault simulations of the 2011 Tohoku, Japan, earthquake. *Bulletin of the Seismological Society of America*, **103**(2B), 1307-1320.

[10] Pan TC, Sun J (1996): Historical earthquakes felt in Singapore. *Bulletin of the Seismological Society of America*, **86**(4), 1173-1178.

[11] Goovaerts P (1997): *Geostatistics for natural resources evaluation*. Oxford University Press: Oxford, New York, 483 pp.

[12] Megawati K, Pan TC, Koketsu K (2003): Response spectral attenuation relationships for Singapore and the Malay Peninsula due to distant Sumatran-fault earthquakes. *Earthquake Engineering & Structural Dynamics*, **32**(14), 2241-2265.

[13] Megawati K, Pan TC (2010): Ground-motion attenuation relationship for the Sumatran megathrust earthquakes. *Earthquake Engineering & Structural Dynamics*, **39**(8), 827-845.

[14] Kohketsu K (1985): The extended reflectivity method for synthetic near-field seismograms. *Journal of Physics of the Earth*, **33**(2), 121-131.

[15] Laske G, Masters G, Reif C (2009): CRUST 2.0: A new global model at 2 x 2 degrees. Institute of Geophysics and Planetary Physics, the University of California, San Diego.

[16] Somerville P, Irikura K, Graves R, Sawada S, Wald D, Abrahamson N, Iwasaki Y, Kagawa T, Smith N, Kowada A (1999): Characterizing crustal earthquake slip models for the prediction of strong ground motion. *Seismological Research Letters*, **70**(1), 59-80.

[17] Schnabel PB, Lysmer J, Seed HB (1972): SHAKE, A computer program for earthquake response analysis of horizontally layered sites. *Report No. EERC 72-12*, Earthquake Engineering Research Center, College of Engineering, University of California, Berkeley.

[18] Vucetic M, Dobry R (1991): Effect of soil plasticity on cyclic response, *Journal of Geotechnical Engineering*, **117**, 89-107.

[19] Kramer SL (1996): *Geotechnical earthquake engineering*. Practice Hall, New Jersey, 653 pp.

[20] British Standards (1997): *Structural Use of Concrete BS 8110*, Part 1, code of practice for design and construction.

[21] Whitman RV, Anagnos T, Kircher CA, Lagorio HJ, Lawson RS, Schneider P (1997): Development of a national earthquake loss estimation methodology. *Earthquake Spectra*, **13**(4), 643-661.